PHYSICAL REVIEW C VOLUME 28, NUMBER 5 NOVEMBER 1983

Optical model description of $\alpha+{}^{16}\text{O}$ elastic scattering and alpha-cluster structure in ${}^{20}\text{Ne}$

F. Michel
Faculté des Sciences, Université de l'Etat, B-7000 Mons, Belgium

J. Albinski
Institute of Nuclear Physics, Krakow, Poland
and Faculté des Sciences, Université de l'Etat, B-7000 Mons, Belgium

P. Belery, Th. Delbar, Gh. Grégoire, and B. Tasiaux
Institut de Physique, Université Catholique de Louvain, B-1348 Louvain-la-Neuve, Belgium

G. Reidemeister
Physique Nucléaire Théorique, CP229, Université Libre de Bruxelles, B-1050 Bruxelles, Belgium

(Received 5 July 1983)

${}^{16}\text{O}(\alpha,\alpha)$ elastic scattering angular distributions have been measured for incident energies 39.3, 49.5, and 69.5 MeV. These data, and previous measurements at 32.2, 104, and 146 MeV, have been subjected to a global optical model analysis. The deduced global potential has two energy-dependent parameters which are found to vary smoothly with energy and it is uniquely determined by the data. Backward angular distributions measured between 40 and 54 MeV are also presented and shown to be nicely reproduced by the model. The sensitivity of the cross sections to the various regions of the real potential has been investigated as a function of energy using the notch test technique. The low energy behavior of the differential cross sections can be understood in terms of the semiclassical decomposition of Brink and Takigawa. A natural extrapolation of the global potential below 30 MeV is shown to reproduce the wide bump observed in the experimental excitation functions around 20 MeV. This bump is shown to be due to an $l=8$ shape resonance and is interpreted as the $J^\pi=8^+$ member of the $K^\pi=0_4^+$ rotational band of ${}^{20}\text{Ne}$, in contradiction with the current attribution. Other bound and quasibound states supported by the potential are discussed in the light of orthogonality condition model-type arguments and shown to be consistent with the well-known $K^\pi=0_1^+$ and 0^- bands, and with the first three states of the $K^\pi=0_4^+$ band of ${}^{20}\text{Ne}$.

NUCLEAR REACTIONS ${}^{16}\text{O}(\alpha,\alpha)$, measured $\sigma(\theta)$, $E_\alpha=39.3$, 49.5, 69.5 MeV; global optical model analysis, $E_\alpha=32-146$ MeV; semiclassical decomposition of the scattering amplitude; investigation of the compatibility of the potential description with existing low energy data and comparison with cluster models.

I. INTRODUCTION

Nucleus-nucleus elastic scattering angular distributions are generally analyzed in the framework of the optical model. At a given energy a local, l-independent potential is often found to give a good description of the experimental differential cross section. It has been known for a long time that this potential is not unique and that the importance of the uncertainties (the so-called "continuous" and "discrete" ambiguities) critically depends on the particular system, the incident energy, the investigated angular range, as well as on the precision of the data. For alpha and helion elastic scattering it has been found possible[1,2] to eliminate the discrete ambiguity on the potential provided the analysis is performed on data taken at a sufficiently high incident energy and extending on a sufficiently broad angular range. For other light projectiles close to the α particle (as, e.g., ${}^6\text{Li}$) the same elimination criteria seem to apply[3] but their extension to heavier projectiles appears to be doubtful.[3,4]

The discrete ambiguities observed at low energy in the scattering of light composite projectiles are often associated with the strongly absorptive character of the potential. However, it is worth pointing out that strong absorption is not a prerequisite for the appearance of ambiguities of this type. Even in the case of proton scattering, which is known as a weak absorption process, it has been demonstrated (at $E_p=10$ MeV in the case of chromium isotopes[5]) that at least two distinct potentials were able to reproduce the scattering data equally well. However, discrete ambiguities have seldom been mentioned for nucleon-nucleus scattering because it was realized very early from theoretical considerations[6,7] that the nucleon-nucleus potential should be about 50 MeV deep; therefore subsequent analyses have been restricted to this potential family. In the case of composite particle scattering the observed ambiguities thus do not necessarily point to a very strong absorption. One of the best examples which illustrates this point is that of $\alpha+{}^{40}\text{Ca}$ elastic scattering for which the discrete ambiguity exists at low energy[8] but where absorption is known to be exceptionally weak as compared with that needed for neighboring nuclei.[9,10] It is possible to resolve this ambiguity by analyzing high energy data where rainbow scattering is observed[11] and to trace the potential from the highest energy ($E_\alpha=166$ MeV) to the low energies ($E_\alpha \approx 20$ MeV). The transparency of the potential allows its precise determination down to very small distances: Notch tests reveal that the scattering is sensitive to modifications of the real potential down to 1—2 fm (Refs. 9 and 12) and likewise a model-independent analysis[8] shows that the error band on the real potential remains narrow down to these distances. It is worth stressing that for most neighboring nuclei such a precise determination of the real potential does not seem to be possible, as the stronger absorption found for these systems leads to much broader error bands.[8] The $\alpha+{}^{40}$Ca potential derived from all these analyses varies smoothly with energy and is able to reproduce the complicated evolution of the experimental differential cross sections on the whole angular range. These qualities, together with the fact that this potential is "unique" and well determined over a wide radial region, indicate that it has a strong underlying physical content and require a microscopic understanding.

A correct description of antisymmetrization is likely to be an essential ingredient of a theoretical description of the system if the scattering is sensitive to rather small interaction distances. The exclusion principle between target and projectile is rigorously taken into account in microscopic approaches such as the resonating group and generator coordinate methods (RGM and GCM).[13—15] The basic ingredients of these methods are fully antisymmetrized wave functions and some nucleon-nucleon effective interaction. It should be kept in mind that simplifying assumptions have to be made on these ingredients (like, e.g., oscillator wave functions for the clusters) in order to make the calculations feasible. A more serious defect of these approaches is that very few channels can be taken explicitly into account (quite often the calculation is restricted to the elastic one) and therefore an empirical absorption is sometimes introduced to simulate the neglected channels and allow a direct comparison with the experimental cross sections. More often comparison with experiment is carried out on energies, widths, and spins of quasibound and virtual levels of the system. The unambiguous determination of these quantities from the data is known to be a delicate problem.[16] On the other hand, the position and width of the calculated levels depend on the particular effective interaction used and could also be affected by the inclusion of previously neglected channels. Therefore a decisive comparison of these microscopic calculations with the experimental data appears to be difficult in many cases.

Promising approaches have recently been proposed to circumvent these difficulties; they consist in building from the complicated RGM kernels real local potentials which predict phase shifts very similar to those generated by a full microscopic calculation.[17,18] These equivalent local potentials are directly comparable to those extracted phenomenologically from optical model analyses. These approaches give an additional impulse to the unambiguous and accurate determination of a potential capable of reproducing the experimental data on the broadest energy and angular ranges for specifically selected couples of nuclei. The systems of doubly closed-shell nuclei are good candidates for that purpose, both from the theoretical point of view, due to the tractability of the calculations, and from the point of view of the phenomenological analysis, as the weaker absorption expected for these systems should allow a precise determination of the potential on a wider radial range.

Returning to the $\alpha+{}^{40}$Ca system, there exists a few calculations in the framework of clusterlike microscopic models [RGM (Refs. 19—24) or shell plus cluster model[25,26]]. Though they all predict low energy states which group into "rotational" bands, they show some differences in the energy position of the bands with respect to the threshold as well as in their degree of splitting. Moreover, the comparison with specific experimental states is complicated by the fact that the spectroscopy of ^{44}Ti is not so well known as that of lighter nuclei, especially above the $\alpha+{}^{40}$Ca threshold. When attempted,[20,27] direct comparison between the predictions of RGM calculations and experimental angular distributions does not help because of the very qualitative nature of the agreement obtained. Therefore we believe that a confrontation of local equivalent potentials derived microscopically, like those built in Refs. 17 and 18, with existing unique $\alpha+{}^{40}$Ca optical potentials[8—10] could be a possible way out for this problem.

Apart from the thoroughly investigated $\alpha+\alpha$ system[28] which would be of little interest in the present context, the only remaining $\alpha+$ doubly closed-shell nucleus candidate is the $\alpha+{}^{16}$O system. The low energy spectroscopy of ^{20}Ne is fairly unambiguous.[29,30] Moreover, this nucleus has been subjected to numerous cluster model investigations.[15] In these calculations the $K^\pi=0_1^+$, 0^-, and 0_4^+ bands are commonly interpreted as unexcited core $\alpha+{}^{16}$O cluster bands; all GCM-RGM calculations, limited to this cluster configuration, carried out with various nucleon-nucleon effective interactions, predict essentially similar phase shift energy behaviors. Unfortunately for ^{16}O(α,α) elastic scattering there exists no systematic optical model analysis comparable to those available for the $\alpha+{}^{40}$Ca system. Most experiments have been restricted to bombarding energies below $E_\alpha \approx 30$ MeV, i.e., to the energy region where prominent structures are observed in the excitation functions; the main purpose of these experiments is to extract spins, resonance energies, and widths of states of the compound system.[31—38] For $E_\alpha \gtrsim 30$ MeV only sparse and/or incomplete angular distributions are available.[39—44]

This prompted us to undertake measurements complementing those few existing above 30 MeV; these new results are presented in Sec. II. These data together with those available above 30 MeV taken from Refs. 42—44 have been subjected to a global optical model analysis, which is presented and discussed in Sec. III. In Sec. IV we show how the extracted potential can be traced down to energies well below $E_\alpha=30$ MeV by analyzing selected angular distributions and by investigating the main trends of existing excitation functions, and we also discuss the significance of quasibound and bound states supported by its real part. Finally we emphasize the general compatibility of our potential with current microscopic ideas. A summary of the main results is presented in Sec. V.

II. EXPERIMENTAL METHOD

The experiment was performed at the Louvain-la-Neuve isochronous cyclotron. The incident α-particle beam was focused at the center of a cylindrical gas cell located in a 1 m diam scattering chamber. Data were taken at four incident energies 31.2, 39.3, 49.5, and 69.5 MeV (the data taken at 31.2 MeV were used to test the compatibility of our measurements with the older data of Cowley and Heymann[43] around 30 MeV). These values correspond to the energies at the center of the gas target. The energy spread of the beam is of the order of 0.3%. The size of the beam spot at the center of the target is about 5×5 mm.

The target gas was chemically pure natural oxygen. The dominant contaminants were xenon (<15 ppm) and argon (<0.4 ppm). The gas cell was made of brass pieces welded and bolted together to form a cylinder 8 cm in diameter and 2 cm useful height. The 320° azimuthal opening was closed by a Havar window 5 μ thick. The gas pressure in the cell was monitored continuously by a calibrated pressure transducer whose output signal was fed in the acquisition system.

The detector system consisted of four silicon detectors 1 mm thick fixed on a turntable rotating around the target cell. The detectors were of the surface-barrier—type except at 69.5 MeV where Si(Li) detectors 3 mm thick were used. In the latter case the turntable temperature was kept at about $-25\,^{\circ}\mathrm{C}$ with a circulation of cold methanol. The detectors were located at 26.8 cm from the center of the target.

For each detector there were two collimators. One brass collimator 0.2 cm wide and 2 cm high was placed at 5 cm from the target cell while a lead collimator was positioned just in front of the detector. It had a thickness of 10 mm and defined an aperture 1 mm wide and 8 mm high. To avoid crosstalk between adjacent detectors, 5 mm thick aluminium plates were mounted radially between the target and the detectors.

A fixed monitor detector was placed at 165° with respect to the beam axis. The accuracy of the detection angles was about 0.1°. The alignment of each pair of collimators was checked with a laser beam.

Each detector amplifier chain was connected to one input of a multiplexer, the output of which was fed into a 1024 channel analog-to-digital converter. The dead time in each chain was monitored continuously with a random pulser. The beam intensity was adjusted to get dead-time corrections less than 10%. The spectra were accumulated in a PDP-8 computer and stored on magnetic tapes for further off-line processing.

The raw angular distributions were obtained by integration of peaks in the spectra. The assignment of peaks was done on the basis of kinematics. Before transformation to the center of mass system, we had to correct the data for multiple scattering in the gas and the window. At each angle we computed the target thickness and effective solid angle. This was done following a procedure outlined by Silverstein.[45]

At the laboratory angle θ, the yield of scattered particles is given by

$$N(\theta)=I_0\frac{N_0G(\theta)}{\sin\theta}\frac{d\sigma}{d\Omega}\ .$$

N_0 and I_0 are the numbers of target nuclei and projectiles, respectively. The factor $G(\theta)$ depends on the geometry and on the angular dependence of the cross section. We chose to evaluate $G(\theta)$ with a Monte-Carlo method instead of performing analytically tedious multiple integrals. The accuracy of our calculations was checked by small angle Rutherford scattering ($\theta_{\mathrm{c.m.}}<30°$) on natural xenon gas. This was done with a 32 MeV alpha particle beam.

In this work we also use $^{16}\mathrm{O}(\alpha,\alpha)$ elastic scattering data obtained as a by-product of a previous experiment.[9] They cover a center of mass angular range from 121.3 to 176.3 deg. The incident energies were 40, 42, 44, 46, 48, 50, and 54 MeV. These old data were normalized to the present ones at 39.3 and 49.5 MeV. The interpolation at other energies was done assuming the energy dependence given by Van Oers *et al.*[39] at $\theta_{\mathrm{c.m.}}=175°$.

III. OPTICAL MODEL ANALYSIS

The $^{16}\mathrm{O}(\alpha,\alpha)$ elastic scattering angular distributions obtained at $E_\alpha=39.3$, 49.5, and 69.5 MeV, together with those previously measured at 32.2, 104, and 146 MeV by the Pretoria,[43] Karlsruhe,[42] and Jülich[44] groups, have been subjected to an optical model analysis. In a first step, individual searches were performed at each energy using various real geometries; because of the well-known insensitivity of the cross sections to the detailed shape of the imaginary potential, the latter was restricted to a squared Woods-Saxon form factor:

$$W(r)=W_0/\{1+\exp[(r-R_I)/2a_I]\}^2\ . \qquad (3.1)$$

Although the familiar discrete ambiguity is present at low energy, from $E_\alpha=69.5$ MeV a single potential family reproduces the experimental data on the whole angular range (we will return to the problem of the uniqueness of the extracted potential at the end of this section). Within this family the resulting potential is found to vary smoothly over the broad investigated energy range: The real part shows little energy variation in the surface region ($r\gtrsim5$ fm), while it displays a systematic decrease in the interior region when energy increases; on the other hand, the parameters W_0 and a_I of the best fit imaginary potentials fluctuate with energy around some average value, while the rms radius $\langle r^2\rangle_I^{1/2}$ shows a systematic increase.

This prompted us to look for some global parametrization of the potential allowing a description of its energy dependence in terms of a minimum number of parameters. It was found that the following flexible parametrization,

$$V(r)=V_0\{1+\alpha\exp[-(r/\rho)^2]\}/\{1+\exp[(r-R_R)/2a_R]\}^2+V_C(r)\ , \tag{3.2}$$

where all the parameters, except α, are kept fixed with energy, is able to reproduce the radial as well as the energy behaviors of the best fit real potentials with good accuracy for the following values of the parameters:

$$V_0=-38\ \text{MeV}\ ,\ \rho=4.5\ \text{fm}\ ,$$
$$R_R=4.3\ \text{fm}\ ,\ a_R=0.6\ \text{fm} \tag{3.3}$$

[note that the real well depth is not given by V_0 but by $V_0(1+\alpha)$]. $V_C(r)$ is the Coulomb potential of a uniformly charged sphere of radius $1.3\times16^{1/3}$ fm. For the imaginary part we kept the parameters W_0 and a_I of Eq. (3.1) fixed at the average values

$$W_0=-25\ \text{MeV}\ ,\ a_I=0.65\ \text{fm}\ . \tag{3.4}$$

All the energy dependence of our global potential [Eqs. (3.1)—(3.4)] is thus contained in the two remaining parameters, α for the real part and R_I for the imaginary part. Finally these two parameters were finely tuned to the data at each energy. At $E_\alpha=104$ MeV the fit obtained gives too low cross sections at small angles as was already observed in the individual best fit; this discrepancy is also apparent in the best fit to the same data obtained by Harakeh *et al.*[46] Moreover, the values of α and R_I we deduced do not come into line with those obtained at the other energies. This could possibly indicate some experimental normalization problem at this energy; indeed adjusting the overall normalization both improves the fit and gives values of α and R_I in better agreement with the general trend (the optimum renormalization of the data is 0.729). The resulting parameters are given in Table I, together with the volume integrals per nucleon pair. The corresponding angular distributions are compared with experiment in Fig. 1. Inspection of Fig. 1 shows that our global potential proves successful in describing the complicated evolution of the angular distribution pattern, including the backward enhancement observed at low energies as well as its progressive disappearance with increasing energy.

The real part of the potential for energies $E_\alpha=32.2$, 69.5, 104, and 146 MeV is plotted in Fig. 2. It can be seen that the nonstandard parametrization of Eq. (3.2) for $V(r)$ does not lead to a peculiar radial dependence of the derived potentials; although simpler form factors could be as successful in representing the data, the energy dependence of Fig. 2 would then require more than a single energy-dependent parameter. The parameter α (Table I) decreases smoothly with energy; in good approximation it can be represented by the linear variation

$$\alpha=3.625-0.0105E_\alpha\ . \tag{3.5}$$

This parametrization is shown in Fig. 3; it corresponds for the real volume integral $J_R/4A$ to the following linear variation:

$$\frac{J_R}{4A}=\frac{J_R^0}{4A}(1-aE_\alpha)\ , \tag{3.6}$$

with $J_R^0/4A=418.1$ MeV fm^3 and $a=0.001\,96$ MeV^{-1}. The value of this last coefficient is close to those extracted phenomenologically for heavier targets[9,47–50] and substantiated by folding model calculations taking into account the nonlocality of the nucleon-nucleus interaction.[47,51] The parameter R_I (Table I) is also shown as a function of energy in Fig. 3. The associated volume integral $J_I/4A$

TABLE I. Best fit values of the parameters α and R_I of the global optical potential [Eqs. (3.1)—(3.4)] obtained at several energies, together with the real and imaginary volume integrals per nucleon pair.

E_α (MeV)	α	$J_R/4A$ (MeV fm^3)	R_I (fm)	$J_I/4A$ (MeV fm^3)
32.2	3.407	399.1	3.122	41.2
39.3	3.125	378.6	3.536	56.4
49.5	3.224	385.3	3.974	76.9
69.5	2.848	357.1	4.382	100.7
104.0	2.374	321.5	4.496	108.3
146.0	2.174	306.5	4.650	119.1

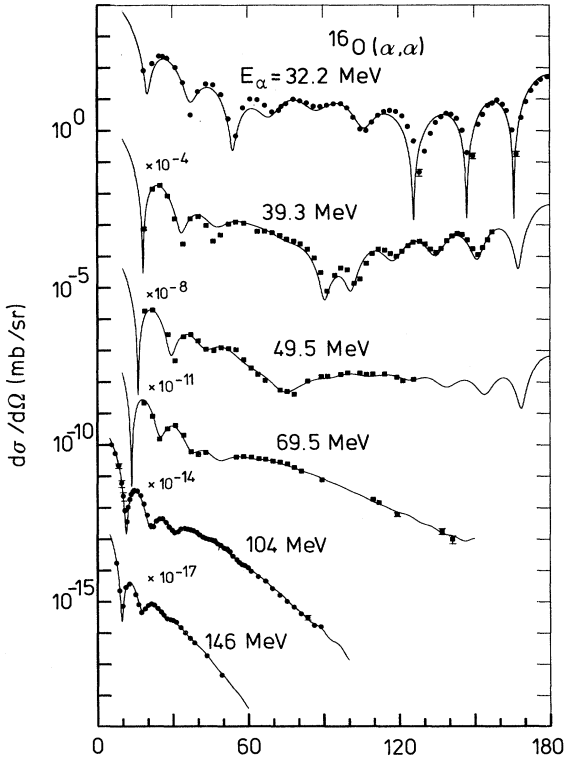

FIG. 1. Comparison of the global optical model cross sections [Eqs. (3.1)—(3.4) and Table I] with experimental angular distributions at 32.2 MeV (Ref. 43), 39.3, 49.5, 69.5 MeV (this work), 104.0 MeV (Ref. 42), and 146.0 MeV (Ref. 44) (the 104 MeV data have been multiplied by 0.729, see text).

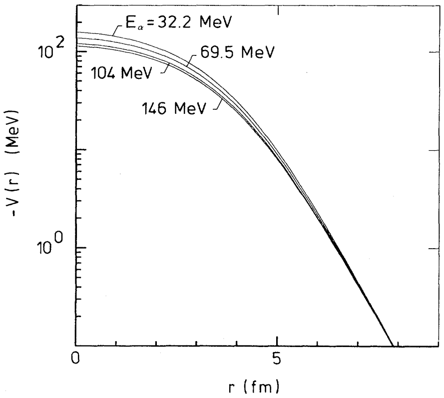

FIG. 2. Real part of the global potential defined by Eqs. (3.1)–(3.4) and Table I, for E_α=32.2, 69.5, 104.0, and 146.0 MeV.

(Table I) increases linearly with energy up to about 50 MeV; this is followed by a slower increase with a tendency to saturation. This behavior is similar to that observed in alpha-particle elastic scattering on heavier nuclei[8,9,49] as well as in proton elastic scattering on various nuclei (see, e.g., Ref. 52).

A measure of the transparency of the derived potential is provided by the so-called "notch test" technique which consists in analyzing the effect of local perturbations of the potential on its ability to describe the data.[12,49,53,54] There exist various ways to perform these modifications; here we chose to perturb the real part of our global potential by multiplying it by the factor

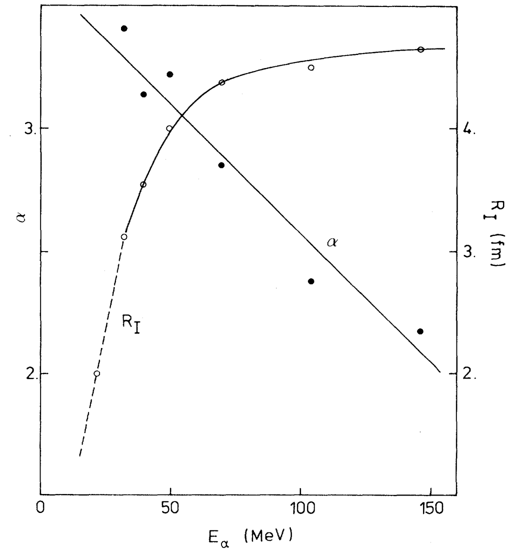

FIG. 3. Energy behavior of the parameters α and R_I of the global potential of Eqs. (3.1)–(3.4): Best fit values (open and closed circles, see Table I); linear approximation of Eq. (3.5) for α (solid line); graphical interpolation for R_I (solid line); linear dependence of R_I used between 15 and 32 MeV [dotted line; cf. Eq. (4.1), see text].

$$f(r;S,b,d)=1-d\exp\{-[(r-S)/b]^2\} , \tag{3.7}$$

where S is varied from 0. to 8.5 fm in 0.5 fm steps. The notch was given a width of about 1 fm by taking $b=0.5$ fm, while its depth was limited to 10% ($d=0.1$). This last value was chosen to avoid excessive modifications of the potential such as those resulting from performing full notches[54] ($d=1$) or cancelling the potential in some range.[53] The effect of the perturbation was judged by evaluating the ratio χ^2/χ_0^2 of the chi-squares corresponding, respectively, to the perturbed and unperturbed potentials. The result of these calculations for E_α ranging from 32.2 to 146 MeV is presented in Fig. 4. This figure shows clearly that, at least for the present system, the scattering is not more sensitive to small distances at high energies than at the lower ones, and therefore it would be wrong to interpret the disappearance of the discrete ambiguity for $E_\alpha \geq 69.5$ MeV as resulting from a transition from diffractive to refractive behavior (cf., e.g., Ref. 55). The scattering is seen to be sensitive to the interaction potential at distances as small as about 2 fm; however, the potential depth at the origin remains completely undetermined at any energy. The most striking energy trends are a slow shift of the maximum of sensitivity to larger dis-

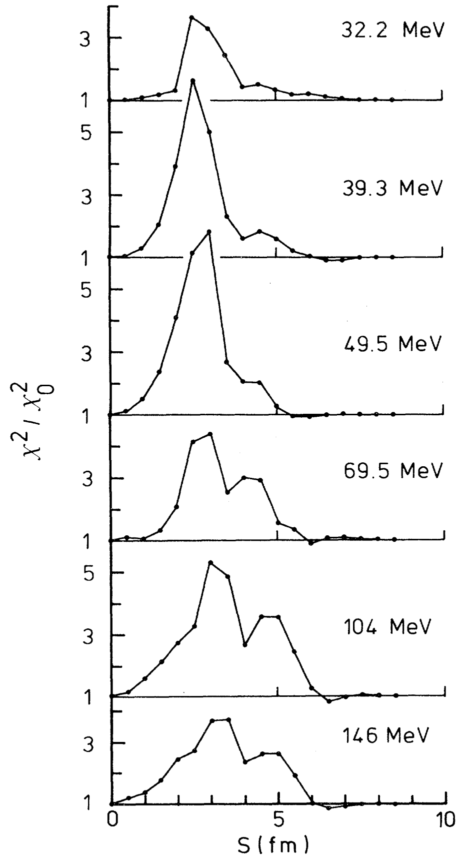

FIG. 4. Ratio of the chi-square obtained after perturbing the potential with a radial notch centered at S to that of the best fits presented in Fig. 1.

tances, and an increase of the sensitivity in the surface region ($r\approx 5$ fm) when energy increases.

Comparison of the predictions of our global potential [Eqs. (3.1)—(3.4)] with the backward angular distributions ($\theta > 120°$) obtained at $E_\alpha=40$, 42, 44, 46, 48, 50, and 54 MeV (see Sec. II) provides an additional test of its ability to describe the data, in a range of energies and/or angles which was not included in the fit. This is the energy range of the transition between the low energy regime, where the backward rise of the cross section is observed, and the high energy regime, characterized by an exponential falloff at large angles. The energy-dependent parameter α was fixed by Eq. (3.5), while R_I was obtained by interpolation from the values given in Table I (the values deduced are, respectively, $R_I=3.59$, 3.68, 3.76, 3.84, 3.91, 3.98, and 4.09 fm for the seven investigated energies). Figure 5 shows that our potential succeeds in predicting quantitatively the typical energy evolution of these experimental cross sections, i.e., the shrinking of the oscillation, the filling up of the minima, and the regular decrease of the slope of the envelope of the maxima.

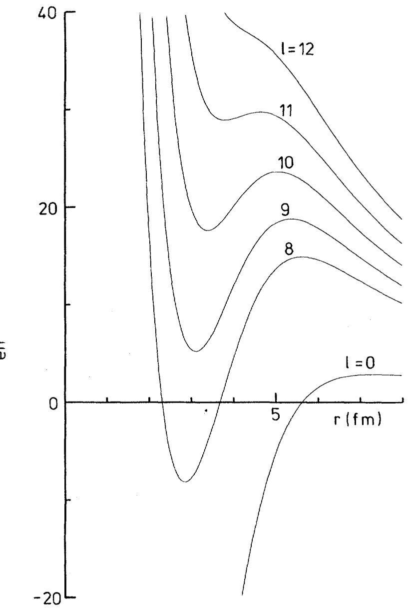

FIG. 6. Effective potentials corresponding to the global potential at 32 MeV defined by Eqs. (3.1)—(3.4) and Table I for $l=0$ and $l=8$—12.

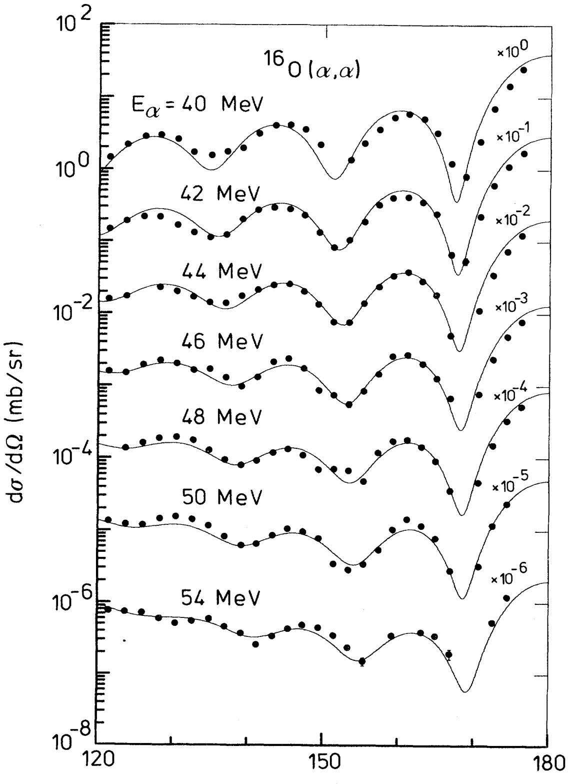

FIG. 5. Comparison of the predictions of the global potential of Eqs. (3.1)—(3.4) [where α is determined by Eq. (3.5) and R_I is taken from Fig. 3] with experimental backward angular distributions at 40, 42, 44, 46, 48, 50, and 54 MeV (this work).

The energy region where this transition occurs coincides with that where the pocket disappears in the effective potential at the grazing angular momentum (i.e., $l\simeq 11$—12, see Fig. 6). For scattering energies below this transition region the semiclassical decomposition of Brink and Takigawa[56] allows the splitting of the elastic scattering amplitude $f(\theta)$ into its barrier and internal components $f_B(\theta)$ and $f_I(\theta)$. These correspond, respectively, to the part of the incident flux reflected by the barrier of the effective potential and that passing the barrier and reflected at the most internal turning point. This decomposition has been carried out at $E_\alpha=32.2$ and 39.3 MeV (with the parameters of Table I) and $E_\alpha=21.5$ MeV (this last energy lies outside the range considered in the global fit; however, it will be shown below that our potential [with α fixed by Eq. (3.5) and $R_I=2$ fm] is still able to reproduce the main trends of the experimental angular distributions at this energy, see Fig. 11). The absolute value of the barrier and internal components of the reflection coefficients, S_B and S_I, is shown in Fig. 7. The corresponding cross sections

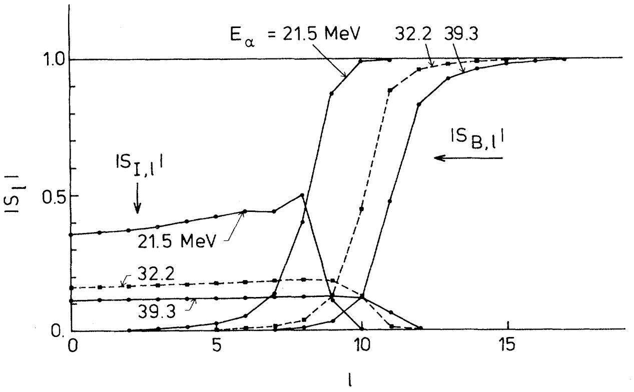

FIG. 7. Modulus of the semiclassical barrier and internal reflection coefficients $S_{B,l}$ and $S_{I,l}$ at $E_\alpha=21.5$, 32.2, and 39.3 MeV calculated with the global potential of Eqs. (3.1)—(3.4); at 21.5 MeV, α is given by prescription (3.5) and $R_I=2$ fm, while at 32.2 and 39.3 MeV α and R_I are taken from Table I.

$$\sigma(\theta)=|f(\theta)|^2\,,\quad \sigma_B(\theta)=|f_B(\theta)|^2\,,$$

and

$$\sigma_I(\theta)=|f_I(\theta)|^2$$

are presented in Fig. 8; the semiclassical cross sections $\sigma(\theta)$ are very similar to the quantal ones at the three energies (compare with Fig. 11 below and with Fig. 1). At small angles the scattering is seen to be dominated by the barrier component, while the internal component accounts for the backward oscillations. This again points to the particular transparency of the ^{16}O(α,α) optical potential, which is reminiscent of that observed in low energy ^{40}Ca(α,α), where a similar mechanism was proved[9,57,58] to be responsible for the large angle enhancement. One sees in Fig. 8 that while the magnitude of σ_B does not change much with energy, σ_I decreases by more than an order of magnitude between 21.5 and 39.3 MeV due to the increase of absorption in the internal region.

For scattering energies near or above the critical energy $E_{\rm crit}^{(1)}$, at which the effective potential loses its pocket at the grazing angular momentum, it still appears possible to distinguish the two components in the quantal S matrix up to a second critical energy $E_{\rm crit}^{(2)}$,[59] noticeably higher than the first one, although the semiclassical method of Brink and Takigawa[56] does no more allow the explicit calculation of these components. The persistency of two contributions above $E_{\rm crit}^{(1)}$ is exhibited by the oscillations observed in the reflection coefficients just below the grazing angular momentum,[59] which are interpreted semiclassically below $E_{\rm crit}^{(1)}$ as resulting from the interference between the two components S_I and S_B.[56] Above $E_{\rm crit}^{(1)}$ these oscillations progressively vanish, and they disappear completely above $E_{\rm crit}^{(2)}$, where the reflection coefficients show a monotonic variation with l. In the present case, our global potential gives $E_{\rm crit}^{(1)}\approx 40$ MeV and $E_{\rm crit}^{(2)}\approx 75$ MeV. [It is worth noting that both critical energies increase with target mass number: For ^{40}Ca(α,α), calculations performed with potential A of Delbar *et al.*[9] give $E_{\rm crit}^{(1)}\approx 50$ MeV and $E_{\rm crit}^{(2)}\approx 105$ MeV, while for ^{90}Zr(α,α) Takigawa and Put[59] find $E_{\rm crit}^{(1)}\approx 80$ MeV and $E_{\rm crit}^{(2)}\approx 165$ MeV.] In the transition region, i.e., for $E_\alpha\approx 40$–50 MeV, the progressive disappearance of the backward enhancement may be associated to the decrease of σ_I due to the persistent increase of absorption. More importantly, the fading of the oscillations in the reflection coefficients at the grazing (see Fig. 9) leads to destructive interference between the successive partial wave amplitudes at back angles. Above $E_{\rm crit}^{(2)}\approx 75$ MeV, where the reflection coefficients behave smoothly with l (Fig. 9), and where the distinction between two components loses any physical meaning, the angular distributions show the typical exponential falloff of rainbow scattering[1,59] (see Fig. 1 and also Fig. 10 below).

We now turn to the problem of the uniqueness of the potential derived in our analysis. As expected, the discrete ambiguity is present at 32.2 MeV, where potentials deeper than our potential [Eqs. (3.1)–(3.4)] turn out to give equally acceptable representations of the data (the first deeper family has $J_R/4A\approx 570$ MeV fm^3; there exists also some evidence for a shallower family, with $J_R/4A\approx 245$ MeV fm^3, which, however, reproduces the data very poorly and cannot be located any more above 32 MeV). The deeper potentials can be traced up to 49.5 MeV, but above that energy they predict angular distributions resembling those observed experimentally at lower energy, in contradiction with the data which show a monotonic decrease with angle. This indicates that our experimental data at 69.5 MeV satisfy the uniqueness criteria of Goldberg and Smith,[1] i.e., that they extend at this

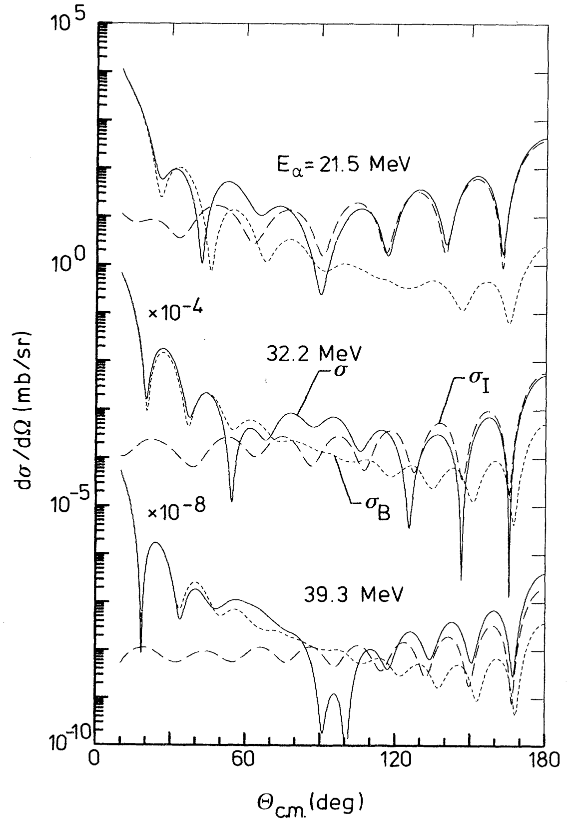

FIG. 8. Semiclassical angular distributions corresponding to the reflection coefficients of Fig. 6 at $E_\alpha=21.5$, 32.2, and 39.3 MeV: Total (full line), barrier (dotted line), and internal (long-dashed line) cross sections.

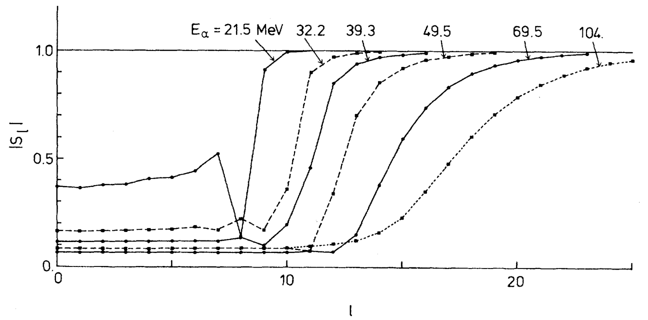

FIG. 9. Modulus of the quantal reflection coefficients S_l calculated with the global potential of Eqs. (3.1)–(3.4); at 21.5 MeV, α is given by prescription (3.5) and $R_I=2$ fm, while at the other energies, α and R_I are taken from Table I.

energy beyond the rainbow angle. In order to check that this is indeed the case, we have calculated the deflection function with the global potential [Eqs. (3.1)–(3.4)] at several energies; the rainbow angles extracted at $E_\alpha=49.5$, 69.5, 104, and 146 MeV are, respectively, $\Theta_R\approx 178°$, 115°, 60°, and 40°. The experimental data are thus seen to extend beyond the rainbow angle at the three highest energies; the 104 MeV data set is the best in this respect: it allows us to assert that our global potential is indeed the unique one, as it reproduces the data equally well at small angles as beyond the rainbow angle (see Fig. 1). This would appear at first sight to be at variance with the results of the analysis performed by Harakeh *et al.*[46] at 104 MeV where potentials belonging to different families seem to give a comparable representation of the data; however, as pointed out in Ref. 46, their potential I, which belongs to the same family as ours, is the only one giving a good fit both to the small angle diffraction pattern and the large angle exponential falloff.

To summarize this section and for illustrative purposes we present in Fig. 10 the predictions of the global potential [Eqs. (3.1)–(3.4)] from 30 to 70 MeV in 2 MeV steps on the whole angular range; α was fixed by prescription (3.5), while R_I was obtained by graphical interpolation from Fig. 3 (full lines). Obviously there is a sharp contrast between the complicated low energy behavior of the cross sections (say, below $E_\alpha\approx 40$ MeV), which is dominated by interference effects between f_B and f_I, especially at midangles, and the much smoother high energy regime where the transition to rainbow scattering is observed, and where the internal wave contribution, although present up to about 75 MeV, plays an ever diminishing role.

IV. DISCUSSION

It is tempting to try to follow the potential below $E_\alpha=32$ MeV, in the region where much structure is observed in the excitation functions[34,36] (we will here restrict ourselves to energies $E_\alpha\geq 15$ MeV). A detailed description of this structure is clearly outside the scope of the optical model: Calculations performed in this energy region with potential (3.1)–(3.4) using values of α and R_I extrapolated from the values obtained above 30 MeV predict only a wide bump around $E_\alpha=20$ MeV.

However, there appears to exist below 32 MeV some "windows" in energy for which the optical model provides a reasonable description of the angular distributions; this is apparent in the work of England *et al.*,[60] where a good optical model description was obtained at 21.5 MeV, and in the orthogonality condition model (OCM) study of Ohkubo *et al.*[61] in the energy range $E_\alpha\approx 21$–24 MeV. Indeed we obtain quite a satisfactory agreement with the experimental angular distribution of Bergman and Hobbie[36] at $E_\alpha=21.5$ MeV with potential (3.1)–(3.4) where α is still fixed by prescription (3.5) and R_I assumes the value 2 fm (see Fig. 11). With the linear dependence,

$$R_I=3.122+0.105(E_\alpha-32.2)\ , \tag{4.1}$$

fixed by the value of R_I just obtained at 21.5 MeV and that obtained at 32.2 MeV (Table I), we next calculate the angular distributions at the energies $E_\alpha=25.4$, 26.6, 28.1, 29.1, 30.0, and 30.9 MeV investigated by Cowley and Heymann[43]; they are compared with experiment in Fig. 12. The overall agreement obtained can be considered as satisfactory in the sense that the essential features of the data, i.e., the evolution of the position of the oscillations and their peak-to-valley ratio, is correctly reproduced. However, the agreement with the experimental pattern at intermediate and backward angles deteriorates at $E_\alpha=28.1$ and 29.1 MeV, i.e., at energies where broad structures are observed in the back angle excitation function.[43,62] The observation of such structures led Cowley and Heymann[43] to analyze their data (from 25.4 to 32.2 MeV) within the frame of a single Regge pole model: In their analysis the scattering amplitude is the sum of a resonant contribution, supposed to be responsible for the large angle enhancement, and of a background contribution, generated by a smooth-cutoff model, which describes the diffractive behavior at small angles. Comparison of Fig. 12 with Fig. 3 from the paper of Cowley and Heymann[43] shows that

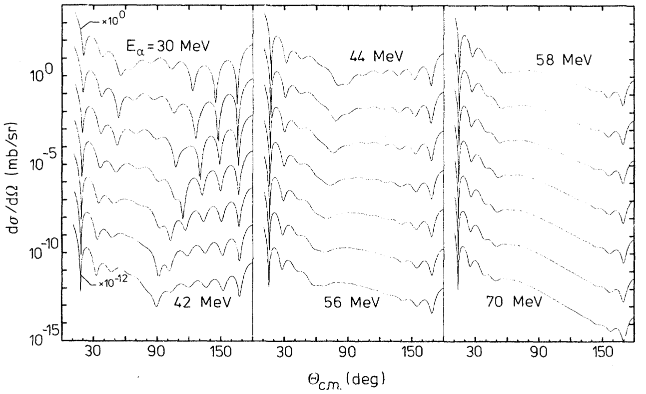

FIG. 10. Predictions of the global potential of Eqs. (3.1)–(3.4) between 30 and 70 MeV in 2 MeV steps; α is given by the linear prescription (3.5), while R_I is graphically interpolated from Table I (see Fig. 3).

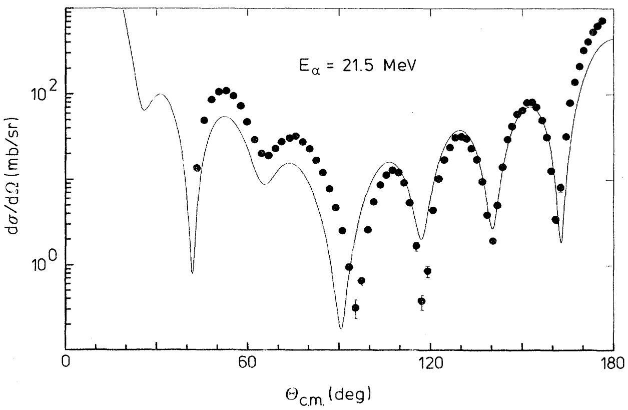

FIG. 11. Comparison of the prediction of the global optical potential of Eqs. (3.1)–(3.5) (with $R_I=2$ fm) with the experimental angular distribution of Ref. 36 at $E_\alpha=21.5$ MeV.

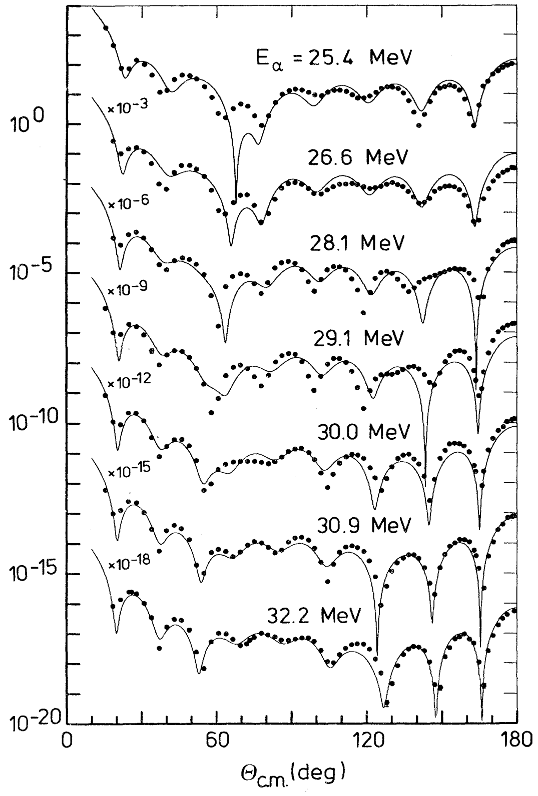

FIG. 12. Comparison of the predictions of the global potential of Eqs. (3.1)–(3.4) with the experimental angular distributions of Ref. 43 between $E_\alpha = 25.4$ and 32.2 MeV; α and R_I are given by prescriptions (3.5) and (4.1), respectively.

the optical potential is nearly as successful as the Regge pole description, but with much fewer energy-dependent parameters. In fact, at 32.2 MeV comparison of Fig. 2 of Ref. 43 with the semiclassical decomposition of our Fig. 8 shows that the Regge pole cross section is very similar to the internal contribution generated by our potential: The Regge pole thus appears to mimic the role of the internal contribution of the potential, not only at 32.2 MeV, but also at the other energies, as evidenced by the similarity of the cross sections predicted by both models down to 25.4 MeV. A closer inspection of the two figures reveals that the discrepancy between the optical model curves and experiment observed at 28.1 and 29.1 MeV in the description of the structure of the back angle oscillations is also present in the Regge pole analysis. Although we could bring the optical model backward angle oscillations in better agreement with experiment by a fine tuning of the imaginary potential parameters, a precise description of these structures seems to require an additional (nonpotential) resonant contribution, which appears to be also missing in the single Regge pole analysis. This casts some doubt on the assignment $J^\pi = 8^+$ proposed by Cowley and Heymann for the 29 MeV resonance.[29,30,43] It should be mentioned in this respect that the analysis of the reaction

$$^{16}\mathrm{O}(^{6}\mathrm{Li},\mathrm{d})^{20}\mathrm{Ne}(\alpha)^{16}\mathrm{O}_{\mathrm{g.s.}}$$

carried out by Artemov *et al.*[63,64] results in the assignment $J^\pi = 10^+$ for the broad structure observed in the d-α coincidence spectrum at the same excitation energy in ^{20}Ne ($E_x = 28.1$ MeV); this structure corresponds in all likelihood to that seen in the elastic scattering, as the d-α coincidence spectrum is known to be highly correlated with the backward $^{16}\mathrm{O}(\alpha,\alpha)$ excitation function.[65] The same assignment 10^+ was also proposed by Bergman and Hobbie[36] from inspection of their elastic excitation functions.

The predictive power as well as the limitations of our potential [Eqs. (3.1)–(3.4)] [extrapolated below 32 MeV with Eq. (4.1)] have been tested further by investigating between 15 and 30 MeV the excitation functions measured[34,36] at several angles in the backward hemisphere. These excitation functions are schematically reproduced in Fig. 13, together with the predictions of the potential (note that the data of Mehta *et al.*[34] seem to have been underestimated by about 40%, as remarked by John *et al.*[35] and more recently by Billen[38]).

The type of "intermediate structure" observed around 28–29 MeV, characterized by widths of about 0.5 to 1 MeV and which is also present at lower energies, is obviously not accounted for by the calculation; in contrast, the potential accounts nicely for the gross structure, a few MeV's wide, observed at some angles around 20 MeV (see Fig. 13), as well as for the overall energy trends with the correct order of magnitude (no attempt was made to improve the agreement by optimizing the potential parameters).

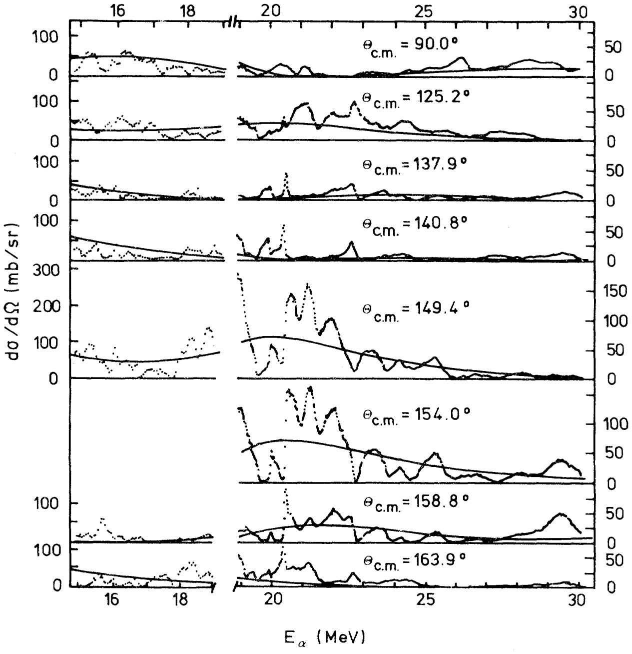

FIG. 13. Comparison of the predictions of the global optical potential of Eqs. (3.1)–(3.4) with the experimental excitation functions of Refs. 33 and 36 between $E_\alpha = 15$ and 30 MeV; α and R_I are given by the linear prescriptions (3.5) and (4.1), respectively.

The origin of this bump may be understood by a closer inspection of the reflection coefficients obtained from the semiclassical decomposition discussed in Sec. III. According to Ref. 58, the internal S matrix S_I may be further split into its single and multiple reflection components,

$$S_I = S_I^{(0)} + S_R \ , \tag{4.2}$$

where $S_I^{(0)}$ corresponds to a single travel of the incident particle inside the effective potential pocket, while the multiple reflections are accounted for by S_R. The contribution of S_R is usually negligibly small, except if absorption is particularly weak. This splitting is presented in Fig. 14 for $E_\alpha = 21.5$ MeV; this energy is located inside the bump and is the lowest energy for which we carried out the decomposition (see Figs. 7 and 8). S_R is seen to be negligible except for $l=8$ (and to a lesser extent for $l=7$ and 9), this contribution being responsible for the small peak observed in $|S_I|$ at $l=8$ ($S_I^{(0)}$ behaves smoothly with l at all energies). We are thus led to associate this bump with a $l=8$ resonance in the entrance channel; this assignment is confirmed by inspection of the corresponding phase shift calculated with the real part of the potential (see below). The same interpretation for this bump also emerged from the OCM study of Ohkubo *et al.*[61] The cross sections σ_I, $\sigma_I^{(0)}$, and σ_R are shown in the backward hemisphere in Fig. 15. The cross sections σ_I and $\sigma_I^{(0)}$ are of similar shape and magnitude, and their oscillations are nearly in phase with those of the square of a Legendre polynomial $|P_7(\cos\theta)|^2$, which is also in phase with the full back angle cross section σ, since the latter is dominated by the internal contribution at these angles. However, it would be misleading (see also Ref. 61) to conclude of the dominance of an $l=7$ resonance: that $l=8$ is indeed the correct assignment can be seen in Fig. 15 where σ_R is seen to be nearly in phase with $|P_8(\cos\theta)|^2$. This example illustrates the pitfalls of the common practice of assigning spins to resonant structures on the basis of Legendre polynomials fits. We also note that it would be incorrect, even at this low energy, to associate the back angle enhancement of the cross section to underlying resonances[43,65] as $\sigma_I^{(0)}$ accounts for most of the effect; at higher energies the sharply increasing absorption makes resonant contributions very small: Indeed, the internal wave reflection coefficients calculated at 32.2 and 39.3 MeV show no trace of the peaking observed at 21.5 MeV (see Fig. 7).

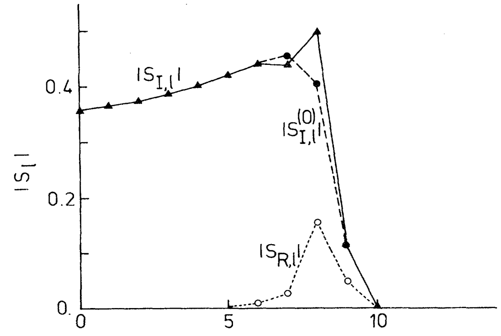

FIG. 14. Decomposition of the semiclassical internal wave reflection coefficients $S_{I,l}$ at $E_\alpha = 21.5$ MeV into their single- and multiple-reflection components $S_{I,l}^{(0)}$ and $S_{R,l}$.

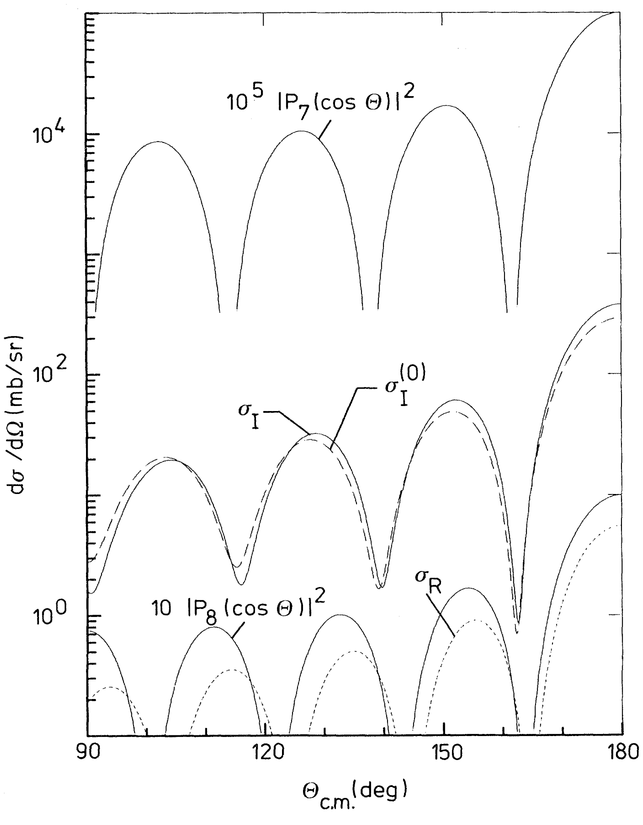

FIG. 15. Comparison of the semiclassical internal-wave cross sections σ_I, $\sigma_I^{(0)}$, and σ_R, corresponding to the reflection coefficients of Fig. 14, with the square of Legendre polynomials of orders 7 and 8.

A deeper understanding of the nature of the broad $l=8$ resonance can be gained by investigating the potential phase shifts, which will at the same time allow us to locate and classify other possible resonances. Since the low-energy behavior of the potential is not precisely known, and rather unessential to the following discussion, the calculations have been performed with the best-fit two-parameter potential obtained at 32.2 MeV (Table I): The resulting phase shifts δ_l, calculated with the real part of this potential, are displayed in Fig. 16 for bombarding energies ranging from 0 to 50 MeV [these are absolute phase shifts, i.e., they tend to zero at infinite energy and are not affected by the usual mod (π) ambiguity]. The figure has been supplemented for negative energies with the bound states supported by the potential down to $E_{\text{c.m.}} = -10$ MeV. The even and odd phase shifts are seen to exhibit markedly different energy behaviors. As expected, δ_8 resonates around 20 MeV incident energy with a width compatible with that of the bump observed in the excitation functions. Clearly each even phase shift up to $l=10$ resonates in turn with increasing positive energy; the same behavior is observed for the odd phase shifts up to $l=9$, but with much smaller widths. Still

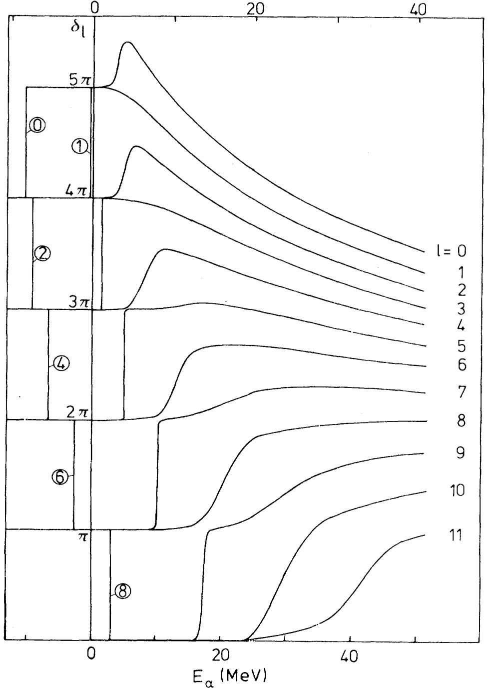

FIG. 16. Bound states and phase shifts calculated with the real part of the 32.2 MeV potential [cf. Eqs. (3.1)—(3.4) and Table I].

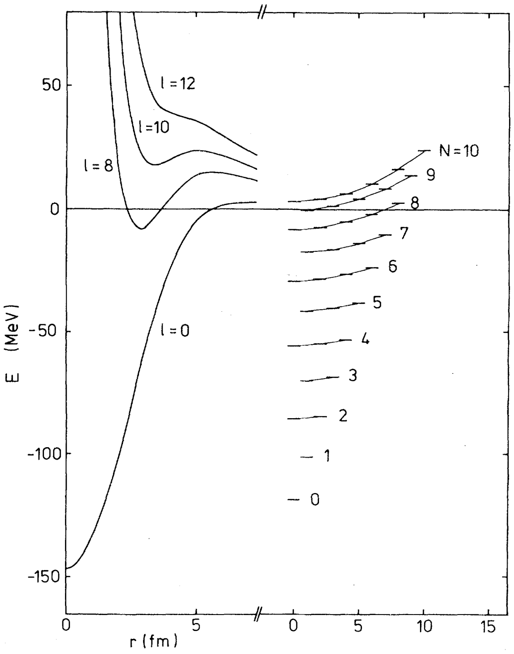

FIG. 17. Bound and quasibound states calculated with the real part of the 32.2 MeV potential; states labeled by the same principal quantum number N are connected by a solid line.

another group of even l states is apparent at negative energies, ending at $l=8$, just above the threshold. In fact, the potential supports many additional bound states (Fig. 17) which group naturally into bands of alternate parities and can be labeled with the principal quantum number $N=2n_r+l$, where n_r denotes the number of radial nodes of the associated wave function.[66,67] The states bound by more than 10 MeV, which do not appear in Fig. 16, correspond in fact to $N<8$, while the three groups of states mentioned above are characterized by $N=8$—10 (an incomplete $N=11$ band of very broad states can also be discerned in Fig. 16 at higher energies).

If we interpret our potential in the spirit of OCM-type approaches,[68–71] which support the use of deep local potentials as a good approximation to full RGM calculations, we are led to discard the states with $N<8$ (simulating the forbidden states of the RGM), and to retain the states with $N \geq 8$ which are the only ones susceptible of a physical interpretation. The first two bands ($N=8$ and 9) must then be interpreted as the members of the "inversion doublet" of ^{20}Ne, and the third one as the "higher nodal band" predicted in RGM-GCM calculations (see Ref. 15 and references therein, and Ref. 72). The experimental states[30] belonging to the $K^\pi=0_1^+,0^-$ bands, which are generally associated with the inversion doublet bands, are displayed in Fig. 18, together with the allowed $N=8$ and 9 states found in our potential; the higher nodal band is often associated[15] with the experimental $K^\pi=0_4^+$ band, whose states[30] are shown on the same figure together with our $N=10$ states. The overall agreement appears to be gratifying, especially if one keeps in mind that these states are calculated with a potential deduced from an analysis of elastic scattering data at much higher energies, i.e., above $E_\alpha \approx 30$ MeV. The $N=8$ band is seen to be shifted downwards by about 4—6 MeV with respect to the experimental ground state band, while the shift of the $N=9$ band is only 1—4 MeV; both calculated bands also appear to be too compressed with respect to experiment. The first states of the $N=10$ band are in very good agreement with those of the experimental 0_4^+ band; this agreement deteriorates for the $J^\pi=6^+$ and 8^+ states. However, the experimental states proposed in Ref. 30 as candidates for the 6^+ and 8^+ members of the $K^\pi=0_4^+$ band (with $E_x=12.58$ and 17.30 MeV, respectively) have far too narrow widths to be compatible with the present analysis. Indeed, our 8^+ state with $N=10$, which is found around $E_\alpha=21$ MeV, is several MeV's wide, i.e., nearly two orders of magnitude wider than that given in Ref. 30; doubt has also been cast on the attribution of the 6^+ state at $E_x=17.3$ MeV to the same band (see Ref. 15, pp. 129—131). In fact all existing RGM-type calculations invariably predict very large widths for the higher members of this band.[61,73–78]

Our potential locates the last member of the $N=10$ band at about $E_\alpha \approx 30$ MeV (see Fig. 16); it manifests itself in this energy region by a very broad plateau in our calculated excitation function at $\theta=180°$. Unfortunately, the existence of this gross structure, which is the last predicted by the potential, cannot be tested experimentally because no detailed excitation function exists above $E_\alpha=30$ MeV.

The results shown on the left-hand side of Fig. 18 were

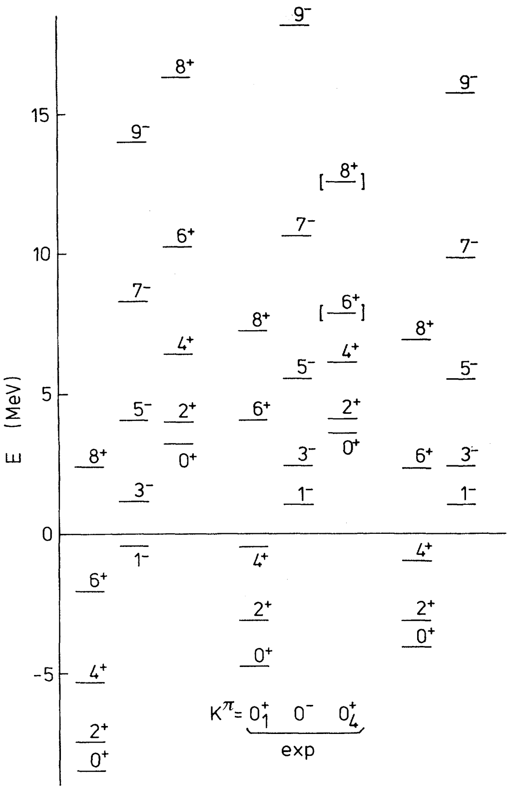

FIG. 18. Comparison of the $N=8$—10 states calculated with the real part of the 32.2 MeV potential (left-hand side) with the experimental $K^{\pi}=0_1^+$, 0^-, and 0_4^+ rotational bands of ^{20}Ne (center) (Refs. 29 and 30); the $N=8$ and 9 bands calculated with $\alpha_+=3.02$ and $\alpha_-=3.21$ are displayed on the right-hand side (see text). The two experimental states appearing between brackets are those whose assignment to the $K^{\pi}=0_4^+$ band is questioned in the text.

obtained with the value $\alpha=3.41$ (i.e., they correspond to the best fit two-parameter potential at $E_\alpha=32$ MeV); it is clear that a consistent use of the prescription (3.5) down to negative energies would worsen the disagreement with experiment for the first two bands, i.e., it would lead to more overbinding. This points to some kind of saturation of the potential depth below $E_\alpha\approx 15$—20 MeV; a similar effect has been reported[8] for the volume integral J_R of the optical potential deduced from a model-independent analysis of ^{40}Ca(α,α). A saturation of the potential depth is also predicted in the recent theoretical analysis of Aoki and Horiuchi[79] based on the deduction of an equivalent local potential from the RGM nonlocal integral kernels [these calculations also predict a decrease of J_R at higher energies, similar to that observed experimentally and mentioned in Sec. III (cf. Fig. 3)]. As a matter of fact, we obtain a better agreement with experiment for the first two bands by slightly readjusting the depth parameter α of the potential; the best agreement is obtained by allowing this parameter to depend on parity. The optimal values $\alpha_+=3.02$ and $\alpha_-=3.21$ were obtained by adjusting, respectively, the calculated 2^+ and 3^- states to their experimental counterparts (a parity effect of comparable magnitude is also reported in Ref. 66). Our resulting $N=8$ and 9 bands are shown on the right-hand side of Fig. 18. The better agreement obtained for the odd parity band is not surprising in view of the fact that it has a more pronounced cluster structure than the ground state band, which appears to be more shell-model—like.[15] The volume integrals per nucleon pair corresponding to α_+ and α_- are, respectively, $J_R^+/4A=369.9$ and $J_R^-/4A=384.1$ MeV fm^3, i.e., significantly lower than the value extrapolated from higher energy [Eq. (3.6)] to the region of the threshold. This deviation remains, however, small as compared with the distance between adjacent families (Sec. III), while the parity splitting appears to be a still smaller effect. This last result is compatible with the conclusions of microscopic investigations, where the parity dependence is found to decrease with increasing mass asymmetry of the system.[80–83]

It is worth closing this discussion of the phase shifts and band structure properties of our potential by noting the great similarity of its real phase shifts (see Fig. 16) and those derived from the numerous RGM and GCM calculations performed so far.[61,73–78]

Finally, we show in Fig. 19 that our 32 MeV potential is nearly identical to the direct potential of Ohkubo *et al.*, which was calculated from the Hasegawa-Nagata-Yamamoto (HNY) effective nucleon-nucleon interaction[61] and was shown in an OCM calculation to describe successfully the band structure and also the elastic scattering data around $E_\alpha\approx 21$—24 MeV. It is also compared with the folding model potential of Buck *et al.*[66] whose depth was adjusted to obtain an optimal description of the first two bands of ^{20}Ne, but was not tested on elastic scattering angular distributions; the somewhat shorter range of this potential, which in all likelihood results from the zero range of their nucleon-nucleon interaction, would probably be a handicap to an optical model analysis at higher energies.

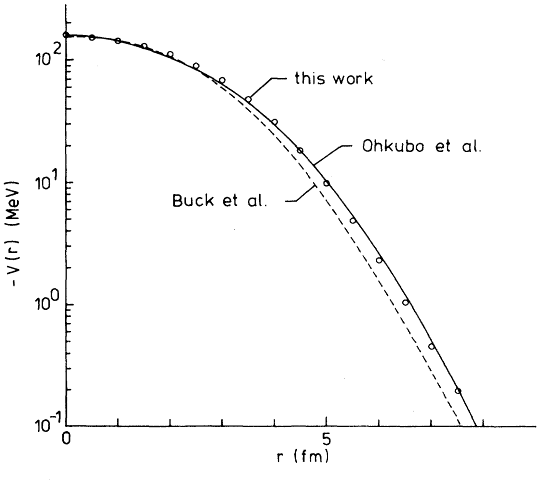

FIG. 19. Comparison of the real part of our 32.2 MeV potential (open circles) with the direct OCM potential of Ohkubo *et al.* (Ref. 61) (solid line) and with the folding model potential of Buck *et al.* (Ref. 66) (dotted line).

V. SUMMARY AND CONCLUSIONS

The compatibility of the phenomenological optical potential deduced from the analysis of extensive elastic alpha-nucleus scattering data with microscopic descriptions of the system has been investigated in the particular case of the α-^{16}O system, which appeared to be the best candidate for that purpose. New elastic scattering measurements were carried out at Louvain-la-Neuve at $E_\alpha = 39.3$, 49.5, and 69.5 MeV. These data, together with previous measurements at 32.2, 104, and 146 MeV, were subjected to a global optical model analysis. The extracted potential, which has only two smoothly varying energy-dependent parameters, gives a precise description of the data on the broad energy range investigated; it also reproduces previous unpublished backward angular distributions measured at Louvain-la-Neuve between 40 and 54 MeV, i.e., in the transition region where the backward enhancement progressively disappears. The sensitivity of the calculated angular distributions to the various regions of the real potential has been investigated as a function of energy using the notch test technique. A semiclassical analysis of the optical model amplitude shows that the complicated energy evolution of the low energy data results from the interference of the barrier and internal wave amplitudes. The available data were shown to allow the elimination of the discrete ambiguity; the real volume integral per nucleon pair of our potential, which is about 400 MeV fm^3 at low energy, decreases with energy with a slope comparable to that found for higher mass targets.

A simple extrapolation of the potential below $E_\alpha = 30$ MeV turns out to provide a natural description of some angular distributions, and of the average excitation functions down to 15 MeV. The broad structure observed at some angles around 20 MeV incident energy is consistently interpreted as the $J^\pi = 8^+$ member of the $K^\pi = 0_4^+$ rotational band of ^{20}Ne, in contradiction with the current attribution,[30] for which this state is located 5 MeV lower and is very narrow. Phase shift and bound state calculations allow to locate lower members of this band, as well as states belonging to two lower bands, which are in good agreement with the well-known $K^\pi = 0_1^+$ and 0^- bands of ^{20}Ne. Lower energy states are discarded by invoking the Pauli exclusion principle between target and projectile through orthogonality condition model-type arguments. The phase shifts and band structure properties of our potential are very similar to those predicted by existing RGM-GCM calculations.

In conclusion, the unique potential deduced from the present extensive analysis of ^{16}O(α,α) elastic scattering data over a broad energy range provides a natural description of the low energy properties of the system, including the band structure of ^{20}Ne. We believe that these properties make it an ideal interface between various experimental aspects of the $\alpha + {}^{16}$O system and their description in terms of microscopic models. The extension of this type of investigation to the $\alpha + {}^{40}$Ca system—where a unique, global optical potential describing elastic scattering on a broad range of energies and angles is available—would probably shed some light on the band structure properties of ^{44}Ti.[84] For elastic heavy ion scattering where the absorption is known to be more important than for alpha-particle scattering, a precise determination of the interaction potential in the interior region could prove impossible. However, the recent observation of back angle anomalies for specific systems,[85] reminiscent of those existing for some alpha-nucleus systems, could point to a certain transparency of the interaction. Whether this transparency will allow an accurate determination of the optical potential for these systems through an extensive analysis of the data remains an open question.

ACKNOWLEDGMENTS

One of us (F.M.) thanks Dr. M. N. Harakeh for sending the numerical values of the Karlsruhe 104 MeV data, and Professor G. J. Wagner for sending his 146 MeV data. F. M. and G. R. thank Professor R. Ceuleneer for his constant interest and his careful reading of our manuscript. J.A. is grateful to Professor R. Ceuleneer for having made possible his stay at the University of Mons, and to the Institut Interuniversitaire des Sciences Nucléaires (IISN) for financial support.

---

[1] D. A. Goldberg and S. M. Smith, Phys. Rev. Lett. 29, 500 (1972).

[2] C. B. Fulmer and J. C. Hafele, Phys. Rev. C 5, 1969 (1972).

[3] R. M. De Vries, D. A. Goldberg, J. W. Watson, M. S. Zisman, and J. G. Cramer, Phys. Rev. Lett. 39, 450 (1977).

[4] M. S. Zisman, J. G. Cramer, D. A. Goldberg, J. W. Watson, and R. M. De Vries, Phys. Rev. C 21, 2398 (1980).

[5] P. T. Andrews, R. W. Clift, L. L. Green, and J.-F. Sharpey-Schafer, Nucl. Phys. 56, 449 (1964).

[6] A. Bohr and B. R. Mottelson, K. Dan. Vidensk. Selsk. Mat.-Fys. Medd. 27, No. 16 (1953), p. 159.

[7] R. K. Adair, Phys. Rev. 94, 737 (1954).

[8] H. P. Gubler, U. Kiebele, H. O. Meyer, G. R. Plattner, and I. Sick, Nucl. Phys. A351, 29 (1981).

[9] Th. Delbar, Gh. Grégoire, G. Paic, R. Ceuleneer, F. Michel, R. Vanderpoorten, A. Budzanowski, H. Dabrowski, L. Freindl, K. Grotowski, S. Micek, R. Planeta, A. Strzalkowski, and K. A. Eberhard, Phys. Rev. C 18, 1237 (1978).

[10] F. Michel and R. Vanderpoorten, Phys. Lett. 82B, 183 (1979).

[11] D. A. Goldberg, Phys. Lett. 55B, 59 (1975).

[12] F. Michel, in *Proceedings of the Karlsruhe International Meeting "What Do We Know about the Radial Shape of Nuclei in the Ca Region?,"* edited by H. Rebel, H. J. Gils, and G. Schatz (Kernforschungszentrum Karlsruhe GmbH, Karlsruhe, 1979), pp. 200—208.

[13] K. Wildermuth and Y. C. Tang, *A Unified Theory of the Nucleus* (Vieweg, Braunschweig, 1977).

[14] Y. C. Tang, M. Le Mere, and D. R. Thompson, Phys. Rep. 47, 167 (1978).

[15] Y. Fujiwara, H. Horiuchi, K. Ikeda, M. Kamimura, K. Kato,

Y. Suzuki, and E. Uegaki, Suppl. Prog. Theor. Phys. 68, 29 (1980).

[16] See, for example, *Proceedings of the Symposium on Resonances in Heavy Ion Reactions,* edited by K. A. Eberhard (Springer, Berlin, 1982).

[17] H. Friedrich, Phys. Rep. 74, 209 (1981).

[18] K. Aoki and H. Horiuchi, Prog. Theor. Phys. 68, 1658 (1982).

[19] H. Friedrich and K. Langanke, Nucl. Phys. A252, 47 (1975).

[20] K. Langanke, Nucl. Phys. A377, 53 (1982).

[21] W. Sünkel, Phys. Lett. 65B, 419 (1976).

[22] A. Tohsaki-Suzuki and K. Naito, Prog. Theor. Phys. 58, 721 (1977).

[23] H. Kihara, M. Kamimura, and A. Tohsaki-Suzuki, in *Proceedings of the International Conference on Nuclear Structure,* edited by T. Marumori (Physical Society of Japan, Tokyo, Japan, 1978), p. 235.

[24] K. Aoki and H. Horiuchi, Prog. Theor. Phys. 67, 1236 (1982).

[25] T. Motoba and K. Itonaga, Suppl. Prog. Theor. Phys. 65, 136 (1979).

[26] K. Itonaga, Prog. Theor. Phys. 66, 2107 (1981).

[27] K. Langanke and D. Frekers, Nucl. Phys. A302, 134 (1978).

[28] J. Hiura and R. Tamagaki, Suppl. Prog. Theor. Phys. 52, 25 (1972).

[29] F. Ajzenberg-Selove, Nucl. Phys. A300, 1 (1978).

[30] F. Ajzenberg-Selove, Nucl. Phys. A392, 1 (1983).

[31] J. R. Cameron, Phys. Rev. 90, 839 (1953).

[32] L. C. McDermott, K. W. Jones, H. Smotrich, and R. E. Benenson, Phys. Rev. 118, 175 (1960).

[33] W. E. Hunt, M. K. Mehta, and R. H. Davis, Phys. Rev. 160, 782 (1967).

[34] M. K. Mehta, W. E. Hunt, and R. H. Davis, Phys. Rev. 160, 791 (1967).

[35] J. John, J. P. Aldridge, and R. H. Davis, Phys. Rev. 181, 1455 (1969).

[36] C. Bergman and R. K. Hobbie, Phys. Rev. C 3, 1729 (1971).

[37] O. Haüsser, A. D. Ferguson, A. B. McDonald, I. M. Szöghy, T. K. Alexander, and D. L. Disdier, Nucl. Phys. A179, 465 (1972).

[38] J. H. Billen, Phys. Rev. C 20, 1648 (1979).

[39] W. T. H. Van Oers, G. J. C. Van Niftrik, H. L. Jonkers, and K. W. Brockman, Jr., Nucl. Phys. 74, 469 (1965).

[40] B. G. Harvey, E. J.-M. Rivet, A. Springer, J. R. Meriwether, W. B. Jones, J. H. Elliott, and P. Darriulat, Nucl. Phys. 52, 465 (1964).

[41] B. G. Harvey, J. R. Meriwether, J. Mahoney, A. Bussière de Nercy, and D. J. Horen, Phys. Rev. 146, 712 (1966).

[42] G. Hauser, R. Löhken, H. Rebel, G. Schatz, G. W. Schweiner, and J. Specht, Nucl. Phys. A128, 81 (1969).

[43] A. A. Cowley and G. Heymann, Nucl. Phys. A146, 465 (1970).

[44] K. T. Knöpfle, G. J. Wagner, H. Breuer, M. Rogge, and C. Mayer-Böricke, Phys. Rev. Lett. 35, 779 (1975).

[45] E. Silverstein, Nucl. Instrum. Methods 4, 53 (1959).

[46] M. N. Harakeh, A. R. Arends, M. J. A. De Voigt, A. G. Drentje, S. Y. Van der Werf, and A. Van der Woude, Nucl. Phys. A265, 189 (1976).

[47] D. F. Jackson and R. C. Johnson, Phys. Lett. 49B, 249 (1974).

[48] P. P. Singh, P. Schwandt, and G. C. Yang, Phys. Lett. 59B, 113 (1975).

[49] L. W. Put and A. M. J. Paans, Nucl. Phys. A291, 93 (1977).

[50] A. Budzanowski, H. Dabrowski, L. Freindl, K. Grotowski, S. Micek, R. Planeta, A. Strzalkowski, M. Bosman, P. Leleux, P. Macq, J. P. Meulders, and C. Pirart, Phys. Rev. C 17, 951 (1978).

[51] F. Duggan, M. Lassaut, F. Michel, and N. Vinh Mau, Nucl. Phys. A355, 141 (1981).

[52] J.-P. Jeukenne, A. Lejeune, and C. Mahaux, Phys. Rev. C 16, 80 (1977).

[53] P. J. Moffa, C. B. Dover, and J. P. Vary, Phys. Rev. C 13, 147 (1976).

[54] J. G. Cramer and R. M. De Vries, Phys. Rev. C 22, 91 (1980).

[55] E. Friedman, H. J. Gils, H. Rebel, and R. Pesl, Nucl. Phys. A363, 137 (1981).

[56] D. M. Brink and N. Takigawa, Nucl. Phys. A279, 159 (1977).

[57] N. Takigawa and S. Y. Lee, Nucl. Phys. A292, 173 (1977).

[58] S. Y. Lee. N. Takigawa, and C. Marty, Nucl. Phys. A308, 161 (1978).

[59] N. Takigawa and L. W. Put, Phys. Lett. 84B, 371 (1979).

[60] J. B. A. England, E. Casal, A. Garcia, T. Picazo, J. Aguilar, and H. M. Sen Gupta, Nucl. Phys. A284, 29 (1977).

[61] S. Ohkubo, Y. Kondo, and S. Nagata, Prog. Theor. Phys. 57, 82 (1977).

[62] A. A. Cowley, S. J. Mills, and G. Heymann, J. Phys. G 4, L149 (1978).

[63] K. P. Artemov, V. Z. Gol'dberg, I. P. Petrov, V. P. Rudakov, I. N. Serikov, and V. A. Timofeev, Yad. Fiz. 23, 489, (1976) [Sov. J. Nucl. Phys. 23, 257 (1976)].

[64] K. P. Artemov, V. Z. Gol'dberg, I. P. Petrov, V. P. Rudakov, I. N. Serikov, V. A. Timofeev, R. Wolski, and J. Schmider, Yad. Fiz. 26, 9 (1977) [Sov. J. Nucl. Phys. 26, 4 (1977)].

[65] K. P. Artemov, V. Z. Gol'dberg, I. P. Petrov, V. P. Rudakov, I. N. Serikov, V. A. Timofeev, and P. R. Christensen, Nucl. Phys. A320, 479 (1979).

[66] B. Buck, C. B. Dover and J. P. Vary, Phys. Rev. C 11, 1803 (1975).

[67] N. Rowley, Phys. Lett. 69B, 25 (1977).

[68] S. Saito, Prog. Theor. Phys. 41, 705 (1969).

[69] V. G. Neudatchin, V. I. Kukulin, V. L. Korotkikh, and V. P. Korennoy, Phys. Lett. 34B, 581 (1971).

[70] V. I. Kukulin, V. G. Neudatchin, and Yu. F. Smirnov, Nucl. Phys. A245, 429 (1975).

[71] B. Buck, H. Friedrich, and C. Wheatley, Nucl. Phys. A275, 246 (1977).

[72] W. Sünkel and K. Wildermuth, Phys. Lett. 41B, 439 (1972).

[73] F. Tanabe and C. Nemoto, Prog. Theor. Phys. 51, 2009 (1974).

[74] T. Matsuse, M. Kamimura, and Y. Fukushima, Prog. Theor. Phys. 53, 706 (1975).

[75] R. A. Partridge, Y. C. Tang, D. R. Thompson, and R. E. Brown, Nucl. Phys. A273, 341 (1976).

[76] M. Le Mere, Y. C. Tang, and D. R. Thompson, Phys. Rev. C 14, 23 (1976).

[77] P.-H. Heenen, Nucl. Phys. A272, 399 (1976).

[78] Y. C. Tang, M. Le Mere, and D. R. Thompson, Phys. Rep. 47, 167 (1978).

[79] K. Aoki and H. Horiuchi, Prog. Theor. Phys. 68, 2028 (1982).

[80] M. Le Mere, R. E. Brown, Y. C. Tang, and D. R. Thompson, Phys. Rev. C 15, 1191 (1977).

[81] M. Le Mere, D. J. Studeba, H. Horiuchi, and Y. C. Tang, Nucl. Phys. A320, 449 (1979).

[82] K. Aoki and H. Horiuchi, Kyoto Report No. KUNS641, 1982.

[83] M. Le Mere, Y. Fujiwara, Y. C. Tang, and Q. K. K. Liu, Phys. Rev. C 26, 1847 (1982).

[84] R. Ceuleneer, F. Michel, and G. Reidemeister, in Ref. 16, p. 227.

[85] P. Braun-Munzinger and J. Barrette, Phys. Rep. 87, 209 (1982).